II International Conference on Particle-based Methods – Fundamentals and Applications
PARTICLES 2011
E. Oñate and D.R.J. Owen (Eds)

MODELLING COHESIVE-FRICTIONAL PARTICULATE SOLIDS FOR BULK HANDLING APPLICATIONS

JOHN P. MORRISSEY, SUBHASH C. THAKUR, JIN SUN, JIAN-FEI CHEN AND JIN Y. OOI

Institute for Infrastructure and Environment
School of Engineering, The University of Edinburgh
The King's Buildings
Edinburgh EH9 3JL
Scotland, U.K
E-mail: J.Morrissey@ed.ac.uk

Key words: Cohesive Solid, Granular Material, Discrete Element Method (DEM), Contact Model, Adhesion.

Abstract. Many powders and particulate solids are cohesive in nature and the strength often exhibits dependence on the consolidation stress. As a result, the stress history in the material leading up to a handling scenario needs to be considered when evaluating its handleability. This paper outlines the development of a DEM contact model accounting for plasticity and adhesion force, which is shown to be suitable for modelling the stress history dependent cohesive strength. The model was used to simulate the confined consolidation and the subsequent unconfined loading of iron ore fines with particle sizes up to 1.18mm. The predicted flow function was found to be comparable to the experimental results.

1 INTRODUCTION

Powders and bulk solids are usually stored and handled in large quantities in many industries. Their constituent particles, varying from nano-particles to grains and ores, differ greatly in size and shape. One common issue for many of these materials is the storage and handling difficulties caused by cohesion. The cohesive strength of a bulk material depends on the consolidation stress it has experienced. As a result, the stress history in the material leading up to a handling scenario needs to be considered when evaluating its handling behaviour. For example, high storage stresses in a silo can lead to high cohesive strength of the stored solid, which may in turn cause blockages such as ratholing or arching near the outlet during discharge.

The discrete element method (DEM) has been extensively used to simulate the behaviour of granular materials. For cohesive solids, it is crucial that the stress history dependent behaviour is adequately captured. A number of contact models are available in several commercial DEM packages to simulate cohesive granular materials. These include the JKR model [1] and capillary force models [2,3]. However, DEM simulations with these models may not capture the stress history dependency behaviour observed in bulk solids.

The paper presents a relatively simple contact model that accounts for plasticity and adhesion forces for use in DEM computation. The predictions using this model for iron ore fines are presented and compared with experimental data.

2 EXPERIMENTAL BEHAVIOUR OF COHESIVE GRANULAR MATERIALS

The flowability of bulk solids, particularly fine grained ones, is greatly affected by the adhesive forces that act between the particles. These forces can be attributed to van der Waals, electrostatic, capillary or magnetic forces to name just a few possible sources and all are dependent on the separation distance of the particles. In moist bulk solids, the capillary forces tend to become the dominant adhesive force, while van der Waals forces become less influential as particle size increases past several microns.

The flowability of bulk solids is usually measured using the flow function, which is the relationship between the unconfined yield strength (σ_c) and the consolidation stress (σ_1). An iron ore fines provided by the Swedish company LKAB was used as the test material in this study to evaluate the capability of the proposed contact model. The flow behaviour was tested physically as described below.

2.1 Test Material

Iron ore fines are the finer fractions (< 6.3mm) that are broken off the main iron ore pellets during handling or storage. The iron ore fines used in this study are from LKAB Direct Reduction (KPRS) pellets and contain particles up to 1.18mm. The material had a bulk density of 2300 kg/m^3 and solid density of 3700 kg/m^3. The behaviour of the iron ore fines is expected to be affected by both the moisture content and the temperature of the sample. Only the effect of moisture content is investigated here. The fines were evaluated at four different moisture content levels: dry (< 0.25%), 1%, 2% and 4%. The moisture content MC was measured by drying a sample in an oven at 105°C for 24 hours.

2.2 Test method

The unconfined stress-strain relationship of the iron ore fine was tested using the Edinburgh Powder Tester (EPT). The EPT is a semi-automated uniaxial tester (Fig. 1), in which the cohesive strength of a bulk solid is evaluated from an unconfined compression test of a material following a period of consolidation to a pre-defined stress level (σ_1). After the removal of the consolidation stress the confining tube is slid off carefully and a vertical force is applied to the sample through the top platen until failure of the sample.

Both the confined and unconfined responses of the iron ore fines were measured. The EPT allows for the evaluation of the bulk compressibility of a material by measuring the height of the sample at incremental consolidation loads. The load is applied to the sample and the sample height is allowed time to stabilise. Once stabilised this is recorded as the consolidated height. Not only can the confined vertical stress-strain response be measured, but also the variation in bulk density during loading, provided the sample mass is known.

During the loading process, the force acting on the top platen, as well as its displacement, are recorded from which the unconfined stress-strain curve can be obtained. The unconfined yield strength (σ_c) is the maximum force recorded during the test. By repeating the

experiment for a range of consolidation stresses the flow function of a bulk solid can be obtained quickly.

Figure 1 - (From left to right) Edinburgh Powder Tester (EPT), confined consolidation, unconfined compression and failed material sample

2.3 Test results

Figure 2 shows the confined stress-strain curves for the iron ore fines at various moisture content levels. The corresponding bulk density variation is shown in figure 3. The results for the dry iron ore fines are not shown as they did not display any cohesive strength up to a consolidation stress of 100 kPa.

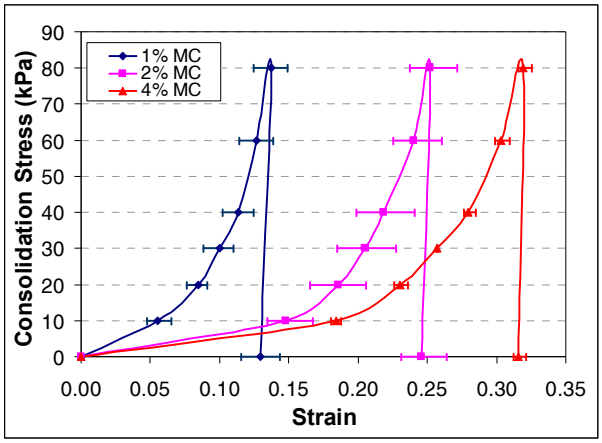

Figure 2 - Stress-strain response during consolidation

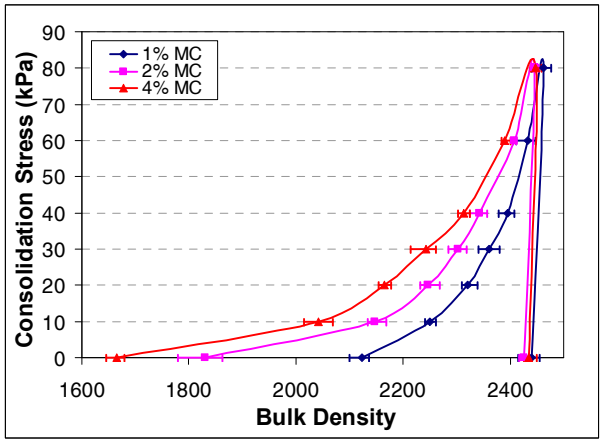

Figure 3 - Bulk density during consolidation

Figure 4 shows the unconfined stress-strain responses for 20, 40, 60 and 80 kPa consolidation (at MC=2%). All the curves show a hardening behaviour initially until failure occurs at the maximum unconfined strength; after that the curves descend, showing a softening behaviour. The unconfined strength increases with the consolidation stress.

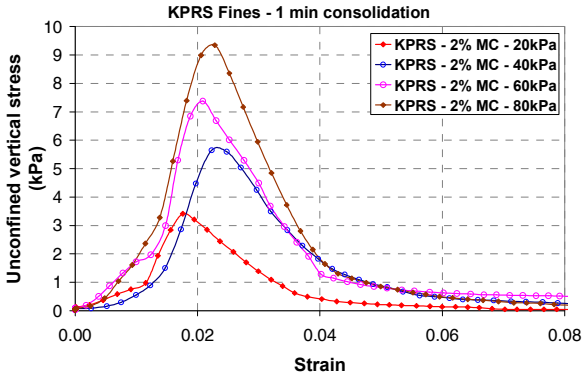

Figure 4 - Stress-strain response for KPRS fines at 2% M.C.

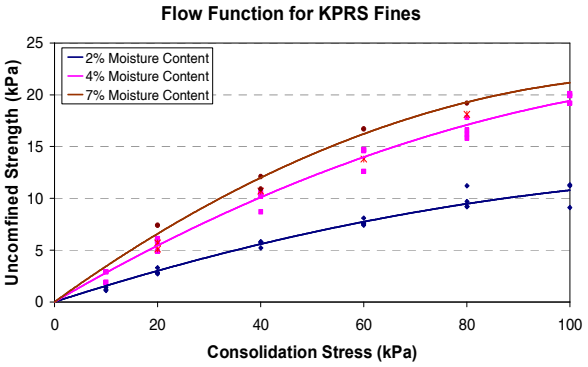

Figure 5 - Flow function for KPRS fines

Once the series of unconfined tests (3-5 tests at each consolidation stress) is complete the flow function can be plotted as the best fit line through the test data. The flow functions for iron ore fines at 2%, 4% and 7% are plotted in figure 5.

3 PARTICLE CONTACT CONSTITUTIVE MODEL

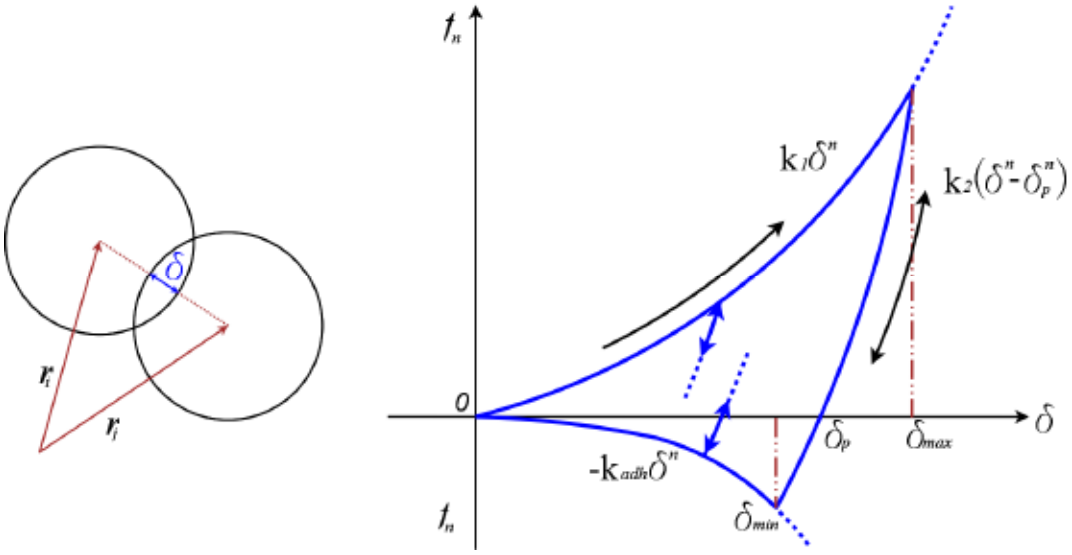

Figure 6 - Proposed contact model

3.1 Visco-elasto-plastic adhesive contact model

A non-linear contact model that accounts for both elastic and plastic contact deformation and adhesion is proposed. The force-overlap (f_{ep}–δ) diagram for this model is shown in figure **6**. The loading, unloading/re-loading and adhesive branches are represented by four parameters: the virgin loading parameter k_1, the unloading and reloading parameter k_2, and the adhesive parameter k_{adh} and the exponent n. The shape of all the three branches is controlled by the parameter n – they all become linear when n=1. Furthermore, if k_1 is set to equal to k_2 the model is reduced to an linear elastic contact model. The normal contact force-overlap

relationship can be mathematically expressed as in Equation 1.

The model reloads initially along the re-loading path k_2 and switches to the virgin loading path k_1 when the previous maximum loading force is reached. Unloading below the plastic overlap δ_p (Fig. 6) results in the development of an attractive force until the maximum attractive force is reached at $-k_{adh}\delta_{min}^{n}$. Further unloading past this point results in a reduction in both the normal overlap and the attractive force until separation occurs.

$$f_{hys} = \begin{cases} k_1\delta^n & if\ k_2(\delta^n - \delta_p^n) \geq k_1\delta^n \\ k_2(\delta^n - \delta_p^n) & if\ k_1\delta^n > k_2(\delta^n - \delta_p^n) > -k_{adh}\delta^n \\ -k_{adh}\delta^n & if\ -k_{adh}\delta^n \geq k_2(\delta^n - \delta_p^n) \end{cases} \quad \textbf{(1)}$$

3.2 DEM implementation

In this study a value of $n=1$ is used which reverts the contact model to a simple linear hysteretic spring contact model accounting for plastic contact deformation [4-10]. In this case Equation 1 is reduced to Equation 2. The adhesion force is linear to the contact deformation and the maximum adhesion force is determined by the stiffness parameters and the maximum normal overlap $\delta_{max,}$ which is recorded and updated over the contact lifetime.

$$f_{hys} = \begin{cases} k_1\delta & if\ k_2(\delta - \delta_0) \geq k_1\delta \\ k_2(\delta - \delta_0) & if\ k_1\delta > k_2(\delta - \delta_0) > -k_{adh}\delta \\ -k_{adh}\delta & if\ -k_{adh}\delta \geq k_2(\delta - \delta_0) \end{cases} \quad \textbf{(2)}$$

The tangential stiffness is calculated based on a constant stiffness k_T, which is set to 2/7 of the normal loading stiffness k_1. The tangential force is calculated from the product of the tangential stiffness and the tangential displacement, subject to the friction limit according to the Coulomb's law. This contact model has been implemented through the API in EDEM® v2.3, a commercial DEM code by DEM Solutions Ltd [11,12]. Custom contact properties are used to record the maximum normal overlaps for contacts.

The default EDEM rolling friction model is adopted in this study.

4 DEM SIMULATION SETUP & RESULTS

The iron ore fines with 2% moisture content were selected as the test material for comparison. A series of uniaxial compression simulations for the test material were conducted using the new contact model. Closely following the EPT physical test procedure, each simulation consisted of three stages – filling the cylindrical mould which formed the initial packing to be used, confined consolidation to the required stress level, followed by unloading, and finally unconfined compression of the sample to failure after the removal of the confining mould.

The details of the simulation setup and parameters are introduced in the next section followed by a discussion of the simulation results.

4.1 Numerical model parameters

A cylinder of 6.5mm radius was filled with 2,500 mono sized spherical particles at 1mm diameter. The random rainfall method was adopted to provide a random packing of particle with a coordination number C≈4. The height of the sample was determined by the filling process in each simulation and was approximately 3-4 times of the radius of the cylinder. Adhesion between particles is accounted for (i.e. with k_{adh} set at an assumed value) in the filling process to allow for the development of a filled porosity similar to the experimental data. If k_{adh} is set to zero, the filling process would produce a highly packed sample with its porosity much lower than the actual material. Large static and rolling friction values were also employed to account for the rough, non-spherical nature of the actual iron ore fines. Values of the parameters used in the simulations are listed in table 1. All parameters were kept constant throughout all simulations.

The cohesive contact model was only applied to particle-particle interactions. The particle-geometry interactions were modelled using the widely used simplified Hertz-Mindlin contact model with no adhesion[13].

The sample was loaded at an axial speed of 5mm/s (strain rate ≈ $0.2s^{-1}$) during the confined consolidation stage and a lower speed of 2.5mm/s (strain rate ≈ $0.125s^{-1}$) during the unconfined compression.

To ensure that all simulations share the same packing structure and loading path (to the required stress levels), the first two stages of filling and consolidation occur in one simulation to the maximum consolidation stress to be considered. Models at each intermediate consolidation stress level were extracted from this simulation and unloaded at the specified consolidation stress, before being loaded to failure as a separate simulation.

Table 1 - Simulation Parameters

Poisson's Ratio, ν	0.3
***Shear Modulus*, G (Pa)**	1.0E+10
***Young's Modulus*, E (Pa)**	2.6E+10
***Particle Radius*, R (m)**	0.0005
***Particle Density*, ρ (kg/m^3)**	4350
***Loading Spring Stiffness, k_1* (N/m)**	1.0E+03
***Unloading Spring Stiffness, k_2* (N/m)**	2.5E+04
***Adhesive Parameter Stiffness, k_{adh}* (N/m)**	6.0E+02
Particle Static Friction, P_{sf}	0.7
Particle Rolling Friction, P_{sf}	0.85
Wall Friction, W_f	0
Base Friction, B_f	0.4
***Simulation Time step* (s)**	1.0E-06

5 SIMULATION RESULTS & DISCUSSION

Figure 7 shows the simulated stress-strain curves for different confined consolidation stress levels. The test results for the iron ore fines at 2% MC are also shown for comparison. The error bars on the experiments represent the range of measured strains in the experiments at each consolidation stress level, for example at 20 kPa the strain varied between 0.165 and 0.2.

The DEM simulations are in a reasonable agreement with the experimental data. The 40 and 60 kPa stress-strain curves lay within the experimental variation at these stress levels, while the 80 kPa is fractionally outside the experimental variation. Only the 20kPa simulation is significantly outside the experimental range by under-predicting the vertical strain. Whilst this simplified contact model has clearly captured some of the non-linear nature of the experimental data, it appeared to predict a bulk response that is too stiff at lower stresses and too soft at higher stresses. Using an exponent value n greater than unity in Eq. 1 can be expected to address this issue.

Much of the non-linearity of the experimental data was related to the rearrangement of the constituent particles. The use of a high rolling friction together with the adhesive forces during filling allowed the simulation to obtain a similar porosity to the iron ore fines. The simulation result had a similar initial softer response that became stiffer as the deformation increased.

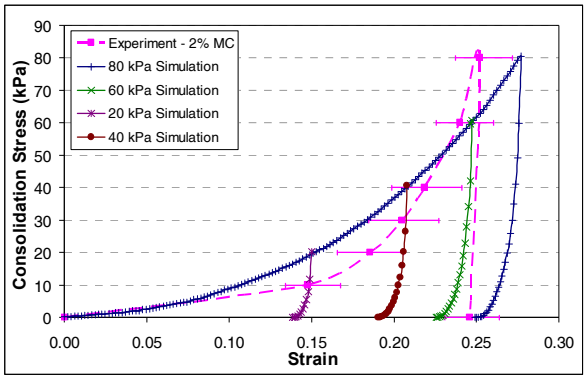

Figure 7 - Axial stress versus strain during confined consolidation

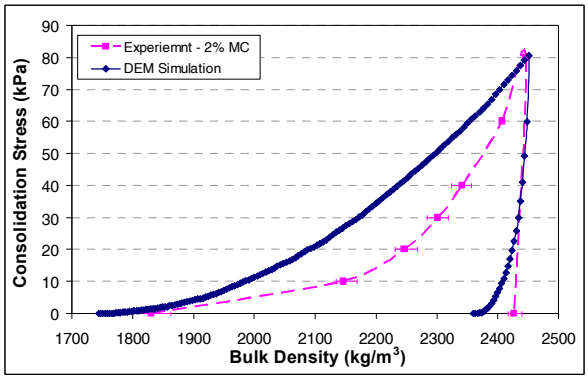

Figure 8 - Bulk density during confined consolidation

The DEM results are compared to the experimental results for bulk density in figure 8 which shows a good agreement in terms of the initial and the maximum consolidated bulk density. The simulated maximum bulk density is 2450 kg/m^3 at a consolidation stress of 80 kPa which is very close to 2440 kg/m^3 measured experimentally at the same stress level. The initial bulk density measured under 3 kPa of consolidation stress in the experiments was 1830 kg/m^3. The corresponding bulk density from the DEM simulation was 1880 kg/m^3. Again the error bars represent the range of bulk densities calculated experimentally at each consolidation stress.

The difference in the bulk density at the end of unloading may be explained by the lack of wall friction in the DEM simulation, allowing a greater elastic rebound of the particles compared to the experimental setup where the friction present between the sample and walls prevented such a rebound occurring. Including friction between particles and the confining cylinder should help to reduce this discrepancy. The issue could also be remedied by increasing the unloading stiffness k_2, but an unloading stiffness of at least an order of magnitude larger would be required and this would reduce the required computational time step and thus increase the total run time significantly.

The difference in the bulk densities at the intermediate stress levels between the

experimental result and the DEM simulation is likely due to the linear nature of the contact model used. A non-linear relationship, similar to that of the Hertzian contact, should provide a much closer match to the non-linear result seen in the experimental data.

The peak strength achieved in each of the simulations is plotted against the consolidation stress giving the flow function in Figure 9. The test results are also plotted for comparison. The flow function calculated from the DEM simulations displays a linear trend, which differs from the nonlinear trend of the test results.

The simulation results provide a closer match to the experimental data at the higher consolidation stresses of 60 & 80 kPa with a much larger deviation occurring at the lower stresses of 20 kPa and 40 kPa. The 80 kPa simulation is the only one that lies within the experimental scatter for unconfined strength and is the only simulation to match the experimental bulk density at that stress level.

Comparing the discrepancy between experiment and simulation, we note that the discrepancy in unconfined strength and bulk density increased in tandem, with the 20 kPa simulation being the furthest from the experimental values. A detailed comparison of the results is presented in table 2 and table 3 below.

Table 2 – Predicted vs test unconfined yield strength (2% M.C.)

Consolidation Stress (kPa)	20	40	60	80
Test: average (kPa)	2.90	5.63	7.64	9.83
Test: COV	0.093	0.051	0.035	0.096
DEM Simulation (kPa)	2.1	4.4	6.9	9.6
% Difference	-27.6%	-21.8%	-9.7%	-2.3%

Table 3 – Predicted vs test consolidated bulk density (2% M.C.)

Consolidation Stress (kPa)	20	40	60	80
Test: average (Kg/m^3)	2250.62	2322.54	2400.85	2422.27
Test: CoV	0.028	0.008	0.010	0.064
DEM Simulation (Kg/m^3)	2085.02	2237.25	2357.11	2447.89
% Difference	-7.4%	-3.7%	-1.8%	1.1%

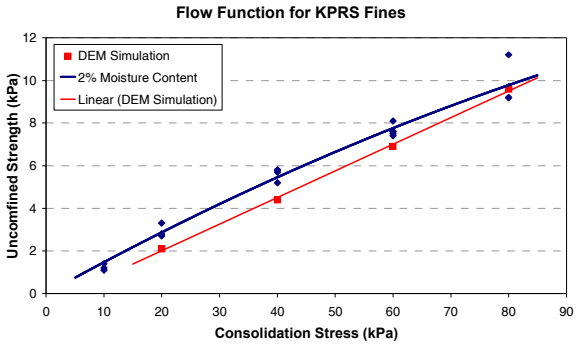

Figure 9 - Experiment-DEM comparison of flow function

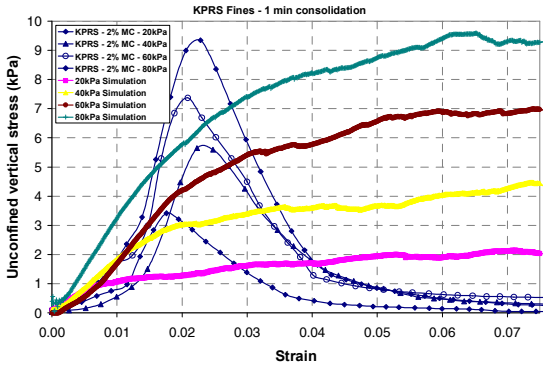

Figure 10 - Stress-strain response comparison

The experimental data shows a clearly defined peak and subsequent drop off in unconfined strength for the iron ore fines that is typical for a material that has been previously over-consolidated (Figure 10). However, the DEM simulations fail to capture this over-consolidation behaviour and instead display a more ductile response, where the peak strength is achieved and maintained for a prolonged strain. Further research is being conducted to investigate this mismatch.

6 CONCLUSIONS

This paper presented a summary of an adhesive elasto-plastic contact model that has been implemented in the commercial DEM code EDEM. Using this new contact model, DEM simulations have been carried out to simulate uniaxial tests on iron ore fines at a moisture content of 2%.

The numerical results have shown that it is possible to simulate the unconfined strength that is dependent on the consolidation stress, which is evident in the experimental data, and hence, to a certain degree match the flow function for iron ore fines. While an exact match to the experimental data has not been achieved yet in terms of the unconfined stress-strain response for iron ore fines, it was found that a reasonable match to the experimental flow function could be achieved. It is also possible to achieve a closer match to the experimental flow function but at the sacrifice of matching the confined consolidation behaviour of the iron ore fines. A parametric investigation is underway to build up a comprehensive understanding of influence of the DEM parameters on predicted bulk behaviour, including introducing a more realistic power law force-displacement relationship. This will underpin the work to derive a robust relationship between the bulk material properties and the contact model parameters.

7 ACKNOWLEDGEMENTS

The authors would like to thank EPSRC, LKAB and DEM Solutions Ltd for the funding and sponsorship. We are also grateful for the discussion with Sten-Evert Forsmo and Kent Tano of LKAB (Sweden), David Curry of DEM Solutions and Geir Horrigmoe of Sweco (Norway).

REFERENCES

[1] Johnson K. L., Kendall K., and Roberts A., 1971, "Surface energy and the contact of elastic solids," Proceedings of the Royal Society of London. Series A, Mathematical and Physical Sciences, **324**(1558), p. 301–313.

[2] Lian G., and Thornton C., 1993, "A theoretical study of the liquid bridge forces between two rigid spherical bodies," Journal of Colloid and Interface Science, **161**, pp. 138-147.

[3] Groger T., Tuzun U., and Heyes D. M., 2003, "Modelling and measuring of cohesion in wet granular materials," Powder Technology, **133**(1-3), pp. 203-215.

[4] Luding S., Tykhoniuk R., and Tomas J., 2003, "Anisotropic Material Behavior in Dense, Cohesive-Frictional Powders," Chemical Engineering & Technology, **26**(12), pp. 1229-1232.

[5] Luding S., 2005, "Anisotropy in cohesive, frictional granular media," Journal of Physics: Condensed Matter, **17**(24), p. S2623-S2640.

[6] Luding S., 2005, "Shear flow modeling of cohesive and frictional fine powder," Powder Technology, **158**(1-3), pp. 45-50.

[7] Luding S., Manetsberger K., and Mullers J., 2005, "A discrete model for long time sintering," Journal of the Mechanics and Physics of Solids, **53**(2), pp. 455-491.

[8] Luding S., 2008, "Cohesive, frictional powders: contact models for tension," Granular Matter, **10**(4), pp. 235-246.

[9] Tomas J., 2009, "Micromechanics of ultrafine particle adhesion–contact models," AIP Conference Proceedings, American Institute of Physics, 2 Huntington Quadrangle, Suite 1 NO 1, Melville, NY, 11747-4502, USA,, p. 781.

[10] Tomas J., 2007, "Adhesion of ultrafine particles—A micromechanical approach," Chemical Engineering Science, **62**(7), pp. 1997-2010.

[11] DEM Solutions Ltd., 2010, EDEM 2.3 User Guide, Edinburgh, Scotland, UK.

[12] DEM Solutions Ltd., 2010, EDEM 2.3 Programming Guide, Edinburgh, Scotland, UK.

[13] Tsuji Y., Tanaka T., and Ishida T., 1992, "Lagrangian numerical simulation of plug flow of cohesionless particles in a horizontal pipe," Powder Technology, **71**(3), pp. 239-250.